PSFC/JA-19-33

3D xRAGE simulation of inertial confinement fusion implosion with imposed mode 2 laser drive asymmetry

M. Gatu Johnson[1] , B.M. Haines,[2] P.J. Adrian,[1] C. Forrest,[3] J.A. Frenje,[1] V.Yu. Glebov,[3] W. Grimble,[3] R. Janezic,[3] J.P. Knauer,[3] B. Lahmann,[1] F.J. Marshall,[3] T. Michel,[3] F.H. Séguin,[1] C. Stoeckl,[3] R.D. Petrasso[1]

[1]Massachusetts Institute of Technology, Cambridge, MA 02139, USA
[2]Los Alamos National Laboratory, Los Alamos, NM 87545, USA
[3]Laboratory for Laser Energetics, University of Rochester, Rochester, NY 14623, USA

December 2019

Plasma Science and Fusion Center
Massachusetts Institute of Technology
Cambridge MA 02139 USA

The authors sincerely thank the OMEGA operations staff who supported this work, Bob Frankel and Ernie Doeg for processing the CR-39, Michelle Evans for characterizing the target glue spots, and Rahul Shah for helpful discussions about framing camera viewing angles. This material is based upon work supported by the Department of Energy, National Nuclear Security Administration under Award Numbers DE-NA0002949 and DE-NA0003868, by the National Laser Users' Facility under award number DE-NA0003938, by LLE under award number 417532-G, and by Los Alamos National Laboratory operated by Triad National Security for the U.S. Department of Energy NNSA under Contract No. 89233218CNA000001. This report was prepared as an account of work sponsored by an agency of the United States Government. Neither the United States Government nor any agency thereof, nor any of their employees, makes any warranty, express or implied, or assumes any legal liability or responsibility for the accuracy, completeness, or usefulness of any information, apparatus, product, or process disclosed, or represents that its use would not infringe privately owned rights. Reference herein to any specific commercial product, process, or service by trade name, trademark, manufacturer, or otherwise does not necessarily constitute or imply its endorsement, recommendation, or favoring by the United States Government or any agency thereof. The views and opinions of authors expressed herein do not necessarily state or reflect those of the United States Government or any agency thereof. Reproduction, translation, publication, use and disposal, in whole or in part, by or for the United States government is permitted.

Submitted to *High Energy Density Physics*

3D xRAGE simulation of inertial confinement fusion implosion with imposed mode 2 laser drive asymmetry

M. Gatu Johnson[1], B.M. Haines,[2] P.J. Adrian,[1] C. Forrest,[3] J.A. Frenje,[1] V.Yu. Glebov,[3] W. Grimble,[3] R. Janezic,[3] J.P. Knauer,[3] B. Lahmann,[1] F.J. Marshall,[3] T. Michel,[3] F.H. Séguin,[1] C. Stoeckl,[3] R.D. Petrasso[1]

[1]*Massachusetts Institute of Technology, Cambridge, MA 02139, USA*
[2]*Los Alamos National Laboratory, Los Alamos, NM 87545, USA*
[3]*Laboratory for Laser Energetics, University of Rochester, Rochester, NY 14623, USA*

Low-mode asymmetries represent an important obstacle to achieving high-gain inertial confinement fusion implosions. As a step in learning how to control such effects, an OMEGA experiment with imposed mode 2 laser drive asymmetries was done to study the expected signatures of this type of asymmetry [M. Gatu Johnson et al., PRE 2018]. In the present work, a 3D xRAGE simulation including the stalk mount has been brought to bear on the data from that experiment. Comprehensive comparisons between simulated and measured observables are made. Good agreement between simulated and measured x-ray image-inferred shell trajectories, bang times and neutron emission widths are seen, showing that the hydrodynamics are well captured in the simulation. Asymmetries seen in simulated and measured time-resolved and time-integrated x-ray images and areal densities also compare well, showing impact of both stalk and mode 2. On the other hand, important differences in measured and simulated neutron emission histories, yield, and ion temperature (T_{ion}) asymmetries are seen, suggesting that the simulation is overestimating shock yield. The results clearly demonstrate the importance of considering all asymmetry sources when interpreting measured signatures of asymmetry.

Keywords: inertial confinement fusion, low-mode asymmetry, radiation-hydrodynamic simulations, neutron spectrometry

1. INTRODUCTION

Inertial confinement fusion (ICF) aims to achieve energy gain by symmetrically imploding a spherical capsule filled with deuterium-tritium (DT) fuel.[1] High implosion performance requires a high degree of symmetry, to allow efficient conversion of shell kinetic energy to thermal energy of the fuel. Low mode asymmetries present a significant challenge to achieving high-performing ICF implosions,[2,3,4] and significant recent work has gone into better understanding the sources and nature of such asymmetries, see e.g. Refs. 5, 6, 7, 8, 9, 10, 11, 12, 13, 14, 15, 16, 17.

As a step in better understanding the signatures of mode 2 asymmetries, a series of implosions was executed at OMEGA with intentional mode 2 laser drive asymmetry imposed at angles intended to maximize the signatures of the mode 2 in directional neutron spectrum measurements. These experiments were described in detail in Refs. 18-19. Signatures in apparent ion temperature (T_{ion}) inferred from neutron spectral broadening, asymmetry inferred from time-resolved self-emission x-ray imaging, and areal density (ρR) asymmetry measurements from these experiments contrasted to 3D Chimera[20] radiation-hydrodynamic simulations not considering the capsule stalk mount strongly suggested that interference between asymmetries seeded by the stalk mount used to hold the capsule and by the imposed

mode 2 had to be considered when interpreting the data.[18,19] This important conclusion will inform interpretation of signatures in experiments with no intentional asymmetry, and improve characterization of implosion asymmetries and their sources going forward. However, missing in this work was a full 3D simulation considering the capsule stalk mount and the imposed mode 2 asymmetry. It would be important to confirm if the observed signatures could be reproduced in simulations considering all the experimental effects.

In this paper, we describe results from a 3D simulation of one of the OMEGA mode 2 implosions using the xRAGE code[21,22,23], which does allow inclusion of the capsule stalk mount in the simulation. Detailed comparisons between simulated and measured observables are made, and the implications of these comparisons are discussed. While many of the observables are captured in the simulations, such as the x-ray and ρR asymmetries, there are also important differences. One important such difference is in the apparent T_{ion} results. The mode 2 signature in the T_{ion} asymmetry is very challenging to model due to its strong dependence on the relative timing of outflow along the asymmetry axis and peak neutron emission; simulations show that the asymmetry flips during the implosion, with higher apparent T_{ion} perpendicular to the imposed mode 2 while the implosion is still converging along all axes and higher apparent T_{ion} parallel to the imposed mode 2 after outflow starts along the asymmetry axis.[19] The differences observed between simulation and experiment lead to one of the most important conclusions of the present work, about shock yield being overestimated in the simulation.

The paper is organized as follows. Section 2 briefly describes the xRAGE simulation, section 3 contrasts experimental and simulated results and discusses implications, and section 4 concludes the paper.

2. 3D XRAGE SIMULATION

The simulation for this paper was done using the radiation-hydrodynamics xRAGE code.[21-23] xRAGE is an Eulerian code which uses adaptive mesh refinement (AMR), making it well suited for modeling the capsule stalk mount. The present xRAGE simulation included hydrodynamics with SESAME tabular equations of state[24], laser ray-tracing using the Laboratory for Laser Energetics' Mazinisin package[25], multi-group radiation diffusion with OPLIB opacities[26], flux limited electronic and ionic thermal heat conduction, a three-temperature (ion, electron, and radiation) plasma treatment, and thermonuclear fusion reactions. xRAGE can be run in 1D, 2D, or 3D. 3D geometry is required to include both the imposed mode 2 and the stalk mount in the simulation, but is computationally expensive, and was thus done only for one of the mode 2 implosions: OMEGA shot 79359. The 3D simulation procedure included an initial 2D laser ray-tracing step. In this step, simulations were performed in 2D with laser ray-tracing including the imposed mode 2 asymmetry. The deposited laser energy was tallied as a function of shell depth and angle at 0.5 μm radial and 0.1° angular resolution, and this was used to drive the 3D simulation as an energy source (similar to the procedure used in Ref. 22). Cross beam energy transfer (CBET), recently shown to be important in modeling of offset implosions,[27] was not directly modeled, but was accounted for by reducing the laser power based on scattered light measurements[19] for these shots. The drive profile for the 3D simulation was modified to account for perturbations due to the 3D beam overlap pattern as well as drive shadowing by the glue on the target mount, so that the energy was deposited into the outer portion of the glue spot instead of the shell. The 3D simulation was performed at a maximum AMR resolution of 0.25 μm, using between 300 million and 6.2 billion computational cells throughout the simulation. Previous resolution studies suggest this resolution is adequate to achieve grid convergence for warm OMEGA implosions (see, e.g., Ref. 22). The simulation was performed on the Knights Landing

partition of Los Alamos National Laboratory's Trinity supercomputer using 24,000 processors and employed a total of 60 million CPU hours.

OMEGA implosion 79359 used an 872-μm outer diameter, 14.5-μm thick CH shell capsule filled with DT^{3}He gas (DT pressure 12.4atm, ^{3}He pressure 7.8atm). All 60 OMEGA laser beams were used with a nominal beam energy of 450 J; the asymmetry was imposed by reducing the energy in two opposing cones of 10 beams each to 315 J, leading to an effective 29% drive asymmetry along the 63.4° polar and 54.0° azimuthal axis. The total laser energy was 22.7 kJ. FIG. 1 shows the xRAGE-simulated 90% gas mass surface (90% of the mass in the cell is gas) for this shot at bang time. The image is colored with thermal T_{ion}. The axis of the imposed mode 2 is vertical in the image, and the stalk enters from the lower right (at 37° to the imposed mode 2). The impact of the asymmetry on the implosion shape can be clearly seen.

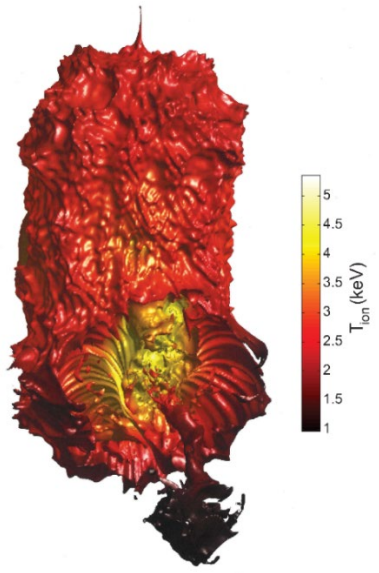

FIG. 1. 3D-xRAGE simulated 90% gas mass surface at bang time color-coded with thermal T_{ion}. The axis of the imposed mode 2 asymmetry is up-down in the image. The stalk enters from the lower right (at 37° to the imposed mode 2). The extent of the image is -83 μm to 101 μm in the up-down direction, and -46 μm to 44 μm and -67 μm to 43 μm, respectively, in the two lateral directions, clearly showing the asymmetry.

3. COMPARISON BETWEEN MEASURED AND SIMULATED RESULTS

In this section, simulated yield, apparent T_{ion}, time-resolved and time-integrated x-ray images, neutron emission history and ρR are contrasted to measurements and the implications discussed. Since the apparent T_{ion} is inferred from the broadening of a measured (or simulated) neutron spectrum, it will include a contribution from thermal T_{ion} as well as a contribution from flow variance in the detector line-of-sight (LOS).[28,29,30] In the present experiment, neutron spectra were measured using the neutron time-of-flight (nTOF) technique. Three detectors were used: two scintillator detectors at 12m and 15.8m from the implosion at polar, azimuthal angles θ=87.8°, φ=161.2° and θ=61.3°, φ=47.6° (henceforth referred to as 12mntof and 15.8mntof) and a CVD diamond detector at 5m from the implosion at θ=85.0°, φ=311.8° (henceforth referred to as 5mcvd).[31,32,33]

Two nominally identical implosions were executed as part of the experiment: shots 79359 vs 79363. While only 79359 was simulated, neutron emission history data and time-resolved x-ray imaging data were only obtained for shot 79363, which means some of the comparisons are done across shots. Implosion and

performance parameters for the two implosions are summarized in Table I. As can be seen, the measured T_{ion} asymmetries were virtually identical for the two shots (see Ref. 19). The bang times were measured with two different detectors for the two shots and are within uncertainty (shot 79359 used an old detector, while 79363 used an improved, lower noise detector[34] which allowed measurement of neutron emission history in addition to bang time). Capsule and laser parameters are also very similar for the two implosions. The yield is higher for 79363; this will be discussed further below. There are two noteworthy differences between shots 79359 and 79363. The first is the difference in glue spot size (see Table I), with 79359 having the larger glue spot. The second is a difference in measured target offset for these two implosions. Offsets are inferred from a system of x-ray pinhole cameras using the method described in Ref. 35. Offsets of 16 μm were inferred for both 79359 and 79363, but with different directions: the offset for 79359 was towards θ,φ=152°,4°, while the offset for shot 79362 was towards θ,φ=140°,209°. Neither of these differences are expected to significantly impact the conclusions, but should be kept in mind when cross-shot comparisons are made.

Table I. Comparison of implosion and performance parameters for nominally identical shots 79359 and 79363.

Shot	DT Yield ($\times 10^{12}$)	Bang time (ns)	Laser energy (kJ)	Capsule outer diameter (μm)	CH shell thickness (μm)	4πΔ wall (μm)	Glue spot length (μm)	Glue spot diameter (μm)	T_{ion} (keV)		
									12mntof	15.8mntof	5.0mcvd
79359	(5.5±0.3)	1.42±0.05	22.7	872	14.5	0.4	97.6	83.1	5.93±0.15	5.89±0.15	5.50±0.17
79363	(8.6±0.3)	1.39±0.05	23.2	870	14.3	0.2	80.9	56.5	5.87±0.15	5.90±0.15	5.54±0.17

In Table II, xRAGE-simulated observables are contrasted to measurements. The first thing to note is that the yield is higher in the simulation, with yield-over-simulated of 52%. The simulated yield is close to the yield for a 2D simulation of this implosion considering just the target mount and no drive asymmetry. The drive asymmetry seems to be diminishing the impact of the target mount in these simulations - the main effect of the target mount is a leakage of fuel and a decrease in pressure in the direction of the target mount, but the asymmetry pushes this away from the center of the fuel region. It is also interesting to note that the measured yield for nominally identical shot 79363 is significantly closer to the simulated yield. As mentioned above, one difference between the two shots is that 79359 has a larger glue spot. However, glue spot size has been previously shown to not significantly impact implosion yield;[12] also, the simulation implements the as-measured glue spot size for 79359. We have recently shown that the angle between any capsule offset and the stalk mount may impact yield,[36] but for these two implosions, this angle (133° and 143°, respectively) and the offset projection in the stalk mount direction (-11 μm and -12 μm, respectively) are very similar. None of the other measured characteristics of shot 79359 can distinguish it from shot 79363, so the additional yield decrease remains a mystery.

Table II. Summary of 3D xRAGE-simulated and measured performance parameters. BWTI is the thermal T_{ion}, not considering flow broadening of the neutron spectrum (this quantity cannot be measured). The experimental T_{ion} values are also contrasted to measurements from a symmetric reference shot to allow inference of the effect of the imposed asymmetry.

	3D xRAGE	Measurement
DT yield	1.06×10^{13}	$(5.5\pm0.3)\times10^{12}$
Bang time (ns)	1.44	1.42±0.05
Neutron emission width (ps)	88	93±5 (shot 79363, corr. for exp. broadening)
Thermal BWTI (keV)	3.76	n/a
12mntof T_{ion} (keV)	5.02	5.93±0.15 (symm ref 5.84±0.15)
15.8mntof T_{ion} (keV)	4.96	5.89±0.15 (symm ref 5.45±0.15)
5mcvd T_{ion} (keV)	4.99	5.50±0.17 (symm ref 5.52±0.33)

The next important thing to study in Table II is the T_{ion} asymmetry. For shot 79359, the 15.8mntof detector was fielded nearly parallel to the imposed mode 2, while the 12mntof and 5mcvd detectors were fielded nearly perpendicular to the imposed mode 2. Experimentally, there is uncertainty in the absolute calibration of each detector relative to the other detectors, so it is important to look at each measurement relative to the T_{ion} measurement using the same detector on a symmetric reference shot. Note that this does not require us to expect the same absolute temperature on the symmetric shot; the comparison is intended to highlight LOS differences between the two shots that must have arisen as the result of the imposed asymmetry. With this in mind, looking at Table II, a significant enhancement in apparent T_{ion} with the imposed mode 2 is seen in the parallel detector, while nearly no difference is seen in the perpendicular detectors. The larger apparent T_{ion} parallel to the imposed mode 2 indicates larger flow variance in this LOS, i.e., that flow is induced along this axis in the implosion. In contrast, minimal LOS variations in T_{ion} are seen in the simulations. This is an interesting difference, which is believed to be due to the challenge in capturing the timing of outflow along the asymmetry axis relative to peak neutron emission in the simulation; this will be discussed further in connection with the neutron emission history discussion below. Note that experimentally, thermal T_{ion} cannot be separated from the flow contribution. This can, however, be done in simulation. Simulated thermal T_{ion}, referred to as burn-weighted ion temperature (BWTI) in Table II, is 3.76 keV, which is 1.3 keV lower than simulated apparent T_{ion} including flow broadening (BWTI is calculated as the neutron emission-averaged thermal temperature). This clearly shows that even though LOS variations are minimal, substantial flows (equivalent to a flow magnitude of ~260 km/s in all directions) are induced in the simulated implosion.

FIG. 2 shows simulated neutron spectra for the 12mntof, 15mntof and 5mcvd lines-of-sight (LOS). It is interesting to note that while minimal LOS variations in T_{ion} are seen between the three detectors, there is a shift in mean energy between the three. Such shifts arise as a result of collective directional flow in the LOS of the observing detector.[37] From the simulated peak energy shifts, directional velocities in each LOS of 9.8 km/s (12mntof), 12 km/s (15.8mntof) and -26 km/s (5mcvd) are inferred. These velocities were inferred by subtracting the zero-temperature mean DT energy and the expected thermal mean energy upshift from the inferred peak energy[38], with the thermal shift calculated for BWTI=3.76 keV (Table II). Unfortunately, the nTOF detectors used in these experiments were not setup with an absolute timing reference, so no absolute peak shifts/directional flows can be obtained from the data. This means that no quantitative conclusions can be drawn from comparison between measurement and simulation, although the measured 5mcvd signal also appears downshifted in energy on shot 79359 qualitatively consistent with the simulated effect.

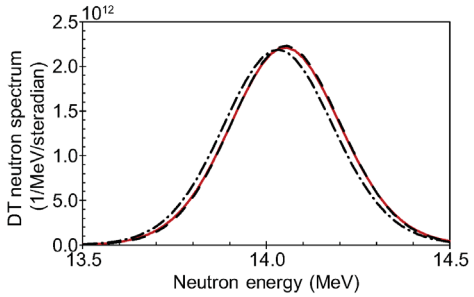

FIG. 2. 3D xRAGE-simulated neutron spectra for the 12mntof (solid red line), 15.8mntof (dashed line), and 5mcvd (broken line) LOS. Note in particular the relative downshift in mean energy for the 5mcvd LOS, corresponding to a simulated 26 km/s directional flow velocity away from this detector.

Implosion shell trajectory (radius versus time) and mode 2 asymmetry amplitude were inferred from time-resolved self-emission x-ray imaging on these implosions using the method described in Ref. 39. Synthetic self-emission x-ray images generated from the simulation allow inference of the same quantities from the simulation. The measured and simulated results are contrasted in FIG. 3. We note that both the radius and the mode 2 amplitude versus time are remarkably well captured in the simulation, suggesting that the overall implosion hydrodynamics are well modeled in the simulation. Also shown in FIG. 3 are the equivalent simulated traces from the 2D xRAGE simulations discussed in Ref. 19, which did not include the capsule stalk mount. In Refs. 18-19, the stalk mount at 37° to the stalk was hypothesized to interfere with the imposed mode 2 to the point of weakening but not eliminating its signature. This hypothesis is supported by the comparison between the 2D and 3D simulated mode 2 amplitudes.

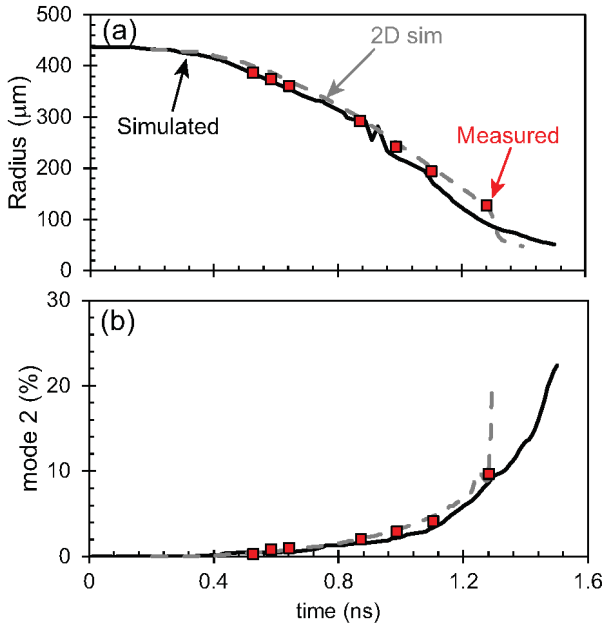

FIG. 3. Comparison of (a) shell trajectory and (b) mode 2 asymmetry amplitude as inferred from simulated (black lines, shot 79359) and measured (red squares, shot 79363) self-emission x-ray images. For comparison, the trajectory and mode 2 inferred from the 2D xRAGE simulations discussed in Ref. 19 are also shown (gray dashed lines). The uncertainty in the measured radii are about 1 μm (smaller than the plotted symbol sizes). The uncertainty in the measured mode 2 is about 0.3% (absolute scale, see Ref. 39).

A subset of the measured and simulated x-ray images used to infer the numbers in FIG. 3 are shown in FIG. 4, with the left column showing simulated images and the right column measured images at comparable times throughout the implosion. The images were obtained at a polar, azimuthal viewing angle θ,φ=37°,162°, which allows observation of 98% of the imposed mode 2 for these shots. The mode 2 asymmetry axis in this projection is indicated with a dashed yellow line in the top panels. Two of the differences between shots 79359 (simulated) and 79363 (measured) discussed above could manifest in these images. The first is the difference in glue spot size, the second the difference in measured target offset for the two implosions. The simulation does not consider a capsule offset, but the offset projection in the x-ray imaging line-of-sight is indicated in both the simulated (79359) and measured (79363) images for reference (red arrows). Both simulated and measured images in FIG. 4 clearly show the signature of the stalk mount. The larger feature in the simulated images could be a result of the larger glue spot on this shot. The white/blue arrows in the top images indicate the initial direction of the stalk mount in this projection. Remarkably, the stalk feature is shifted slightly relative to this initial direction in a nearly identical way in

the simulated and measured images. Analysis of the simulation shows that the apparent position of the stalk moves by about 7° due to interaction with drive asymmetry between its initial location and its location at bang time.

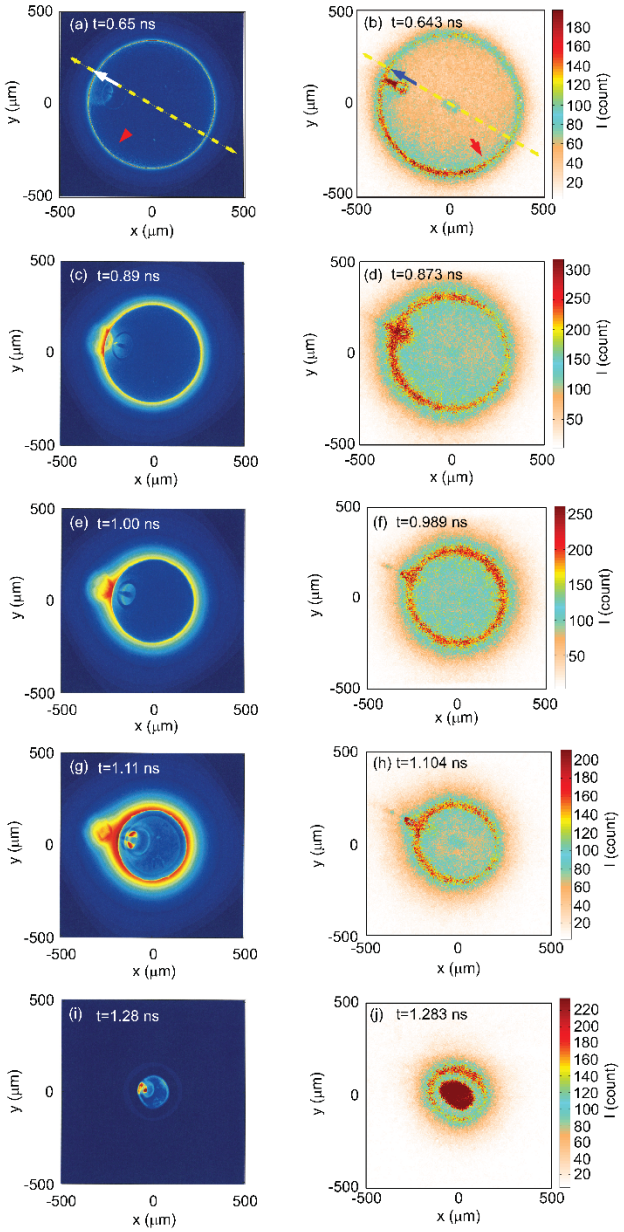

FIG. 4. Simulated (shot 79359; a, c, e, g, i) and measured (shot 79363; b, d, f, h, j) self-emission x-ray images as a function of time. The glue spot was larger for shot 79359 (diameter 83 μm, length 98 μm) than for shot 79363 (diameter 57 μm, length 81 μm), which means we do expect some differences in the appearance of the stalk perturbation between simulation and measurement. In the top panels, the white/blue arrows indicate the direction of the stalk mount, the dashed yellow line the axis of the mode 2 asymmetry (which coincides with the stalk in this projection but is 37° away from the stalk in 3D), and the red arrow the measured target offset in this projection.

FIG. 5 shows time-integrated x-ray images obtained with the GMXI diagnostic[40]. These images are more heavily filtered than the time-resolved images, meaning they are weighted towards higher energy x-ray emission and thus see more core and less shell emission compared to the images in FIG. 4. GMXI is fielded at θ,φ=96°,54°, and will only see 54% of the imposed asymmetry for shot 79359. The

experimental image shown in FIG. 5a exhibits unambiguous signatures of the mode 2 asymmetry (a fit to the 30% intensity contour gives an average radius of 37 μm and a mode 2 amplitude of 21%). In FIG. 5a, the mode 2 axis (dashed yellow line), stalk angle (white arrow) and the offset projection (red arrow) in the GMXI view are also shown. It is interesting to see that the experimentally measured asymmetry does not exactly follow the mode 2 axis; it appears tilted towards the stalk direction, with the observed mode 2 asymmetry falling between the imposed mode 2 axis and the stalk axis. Also shown in FIG. 5 is a synthetic time-integrated x-ray image generated from the xRAGE simulation. The simulated image has has had a 10 μm spatial smoothing applied. Temporally, it is a sum of individual images with 10 ps spacing; the strong structure in the image may be an artifact of the high-intensity feature only appearing in a single one of these time slices. The mode 2 asymmetry is clearly seen also in the synthetic image. Interestingly, the simulated x-ray image exhibits a larger hot spot than the experiment, despite having similar trajectories to ~1.3ns (FIG. 3). The radius inferred from the 30% contour is 61 μm. This is currently believed to be due to the imploded material staying artificially hot as it expands in the simulation. (For implosions, it is common to use a diffusion approximation that assumes a scattering-dominant medium, and this assumption does not hold in the low-density blow-off region. This means that hot carbon on the outside of the fuel region may not cool efficiently enough, which could stretch out the emission through disassembly).

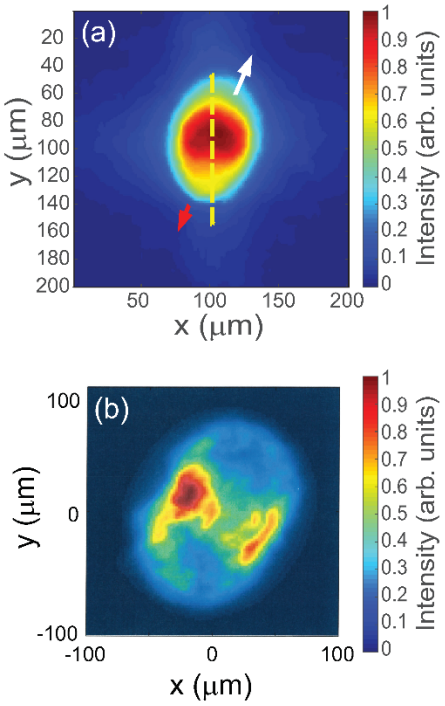

FIG. 5. Time-integrated x-ray images, filtered to emphasize core emission. (a) Measured time-integrated x-ray image from shot 79359, compared to (b) a synthetic image from the simulation with the same viewing angle and rotation. These images see 54% of the imposed mode 2 asymmetry.

It is instructive to compare simulated and measured neutron emission histories. From Table II, we note that simulated and measured bang times agree within the experimental uncertainty, as do the neutron emission widths. Note that the experimental width in Table II has been corrected for experimental broadening, including the detector impulse response 40±10 ps, the neutron transit time through the scintillator 20 ps, and the thermal broadening of the DT neutron spectrum.[34] To allow for a direct comparison, FIG. 6 shows simulated and measured neutron emission histories aligned by the respective

bang times, with the simulated trace folded with the experimental broadening. Note that no yield normalization has been done for this plot; the simulated total yield of 1.06×10^{13} and the measured yield for shot 79363 of 8.6×10^{12} are reflected in the traces. The most obvious difference is that the simulated trace has a small peak ~200ps before bang time that is absent in the experimental data; this seems to be where most of the yield discrepancy arises. This yield corresponds to shock flash yield in the simulation, and suggests that the simulation could be over-predicting the ion heating at shock flash. This potentially points to an issue with how energy deposited by shocks is modeled, which could be an important result. A possible explanation is that this is because the simulation neglects electron viscosity, and hence over-estimates the fraction of shock energy that gets deposited into the ions. This idea was proposed in Ref. 41.

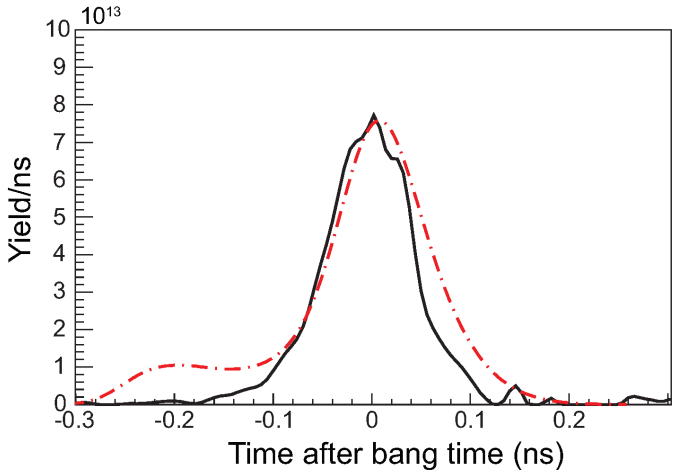

FIG. 6. Comparison of simulated (broken red curve, shot 79359) and measured (solid black curve, shot 79363) neutron emission histories. The curves have been aligned to the respective bang times; simulated and measured bang times agree within error bar as can be seen in Table II. The simulated neutron emission history has been folded with the experimental response as detailed in the text to allow direct comparison of the traces.

Returning to the discussion about LOS differences in T_{ion}, it is also interesting to study how apparent T_{ion} evolves in time in the simulation. FIG. 7 shows the simulated apparent T_{ion} as a function of time for the three nTOF LOS used in the experiment: 12mntof and 5mcvd approximately perpendicular to the imposed mode 2, and 15.8mntof approximately parallel to the imposed mode 2. Also overlaid in FIG. 7 is the simulated neutron emission history. FIG. 7 shows that before peak neutron emission, higher T_{ion} is seen perpendicular than parallel to the imposed mode 2. This is because the implosion is still compressing along all axes at this time; with the stronger laser drive perpendicular to the imposed mode 2, the induced flow variance is stronger along this axis. After peak neutron emission, the asymmetry flips, with higher T_{ion} now seen parallel to the imposed mode 2. This is because at this point, outflow starts along the asymmetry axis. This gives rise to a larger flow variance in this direction compared to the perpendicular direction. In the simulation, virtually no net difference averaged over neutron emission is seen in apparent T_{ion} between the three viewing directions (Table II). However, if the apparently artificial shock neutron emission early in the neutron emission history is eliminated (cf. FIG. 6), the weighting shifts to the outflow time contributing more to the neutron emission-averaged T_{ion}. Numerically, applying a ramp to eliminate shock neutron emission and re-averaging the T_{ions} gives 4.42 keV and 4.41 keV for 12mntof and 5mcvd, respectively, while it gives 4.57 keV for 15.8mntof, i.e., higher T_{ion} parallel to the imposed mode 2 consistent with the measurements (although we note that the absolute T_{ion} in this case is further from the measured values).

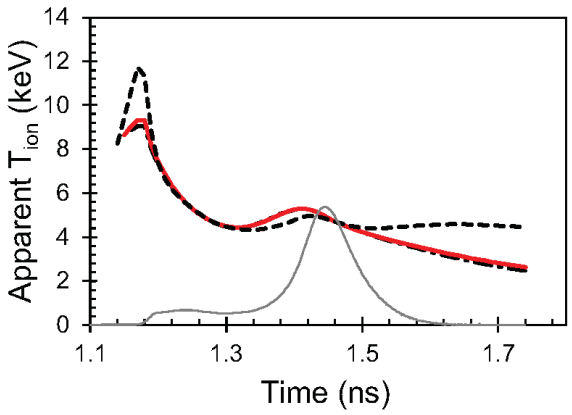

FIG. 7. Simulated apparent T_{ion} as a function of time for the three different nTOF detectors used in the experiment. The detectors fielded nearly perpendicular to the imposed mode 2 (12mntof, 5mcvd, solid red and broken black lines) show the highest T_{ion} early in the pulse (before bang time), while the detector fielded parallel to the imposed mode 2 (15.8mntof, dashed black line) shows the highest T_{ion} late in the pulse, after outflow has started along the asymmetry axis. The simulated neutron emission history is also shown for reference (arbitrary amplitude, solid gray curve).

Finally, it is also interesting to study ρR. FIG. 8a shows the simulated neutron emission-averaged ρR vs angle (note that the apparent lines to the left and right in the image are artifacts of the reprojection[a]). There is a clear impact of the imposed mode 2, with lower ρR in the regions of lower drive (the centers of the reduced-drive cones are indicated with blue plus signs in this plot). Experimental ρR was inferred from downshifts of measured D^3He-proton spectra on this implosion using proton spectrometers in five different LOS: the magnetic recoil spectrometer[42] (θ,φ=119°,308°), two charged particle spectrometers[43] (with θ,φ=63°,198° and θ,φ=37°,18°), and two wedge range filter spectrometers[44] (fielded at θ,φ=63.4°,342.0° and θ,φ=58°, 54°). The measured data is contrasted to simulation in FIG. 8b. Good general agreement is seen, although simulated ρR is lower than measured on average. At first glance, it appears that the drive asymmetry is dominating the ρR variation, because the weak point in FIG. 8a (at ~θ,φ=70°,20°) is not aligned with the initial location of the stalk (red cross in FIG. 8a). However, a closer comparison with simulation indicates that the drive asymmetry has the effect of distorting the apparent location of the weak spot generated by the stalk. This can be understood by looking at FIG. 1 - imagine where the weak point (at the bottom right of the image) would be if the fuel region was spherical and not prolate. As a result, the ρR measurements are taken further from the location of the target mount than expected. This could also mean that the target mount has a much bigger impact than expected on the LOS variations because the apparent stalk location is much closer to one of the detectors than its initial orientation would indicate.

[a] The simulation was done with the drive asymmetry aligned with the z-axis and the plot is done relative to up-down in the target chamber. The ρR was sampled uniformly in angle in the xRAGE frame of reference, and these lines correspond to θ=0° and φ=360° in the source projection. The small cells at this interface get stretched during reproduction, so that a source "cell" is stretched over several destination "cells" in the reprojection. This results in interpolations that no longer exactly line up.

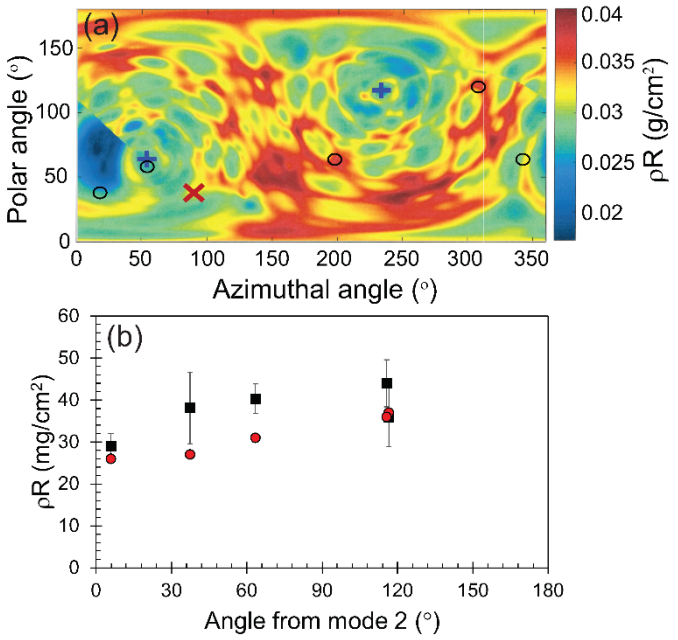

FIG. 8. ρR distribution. (a) Simulated neutron emission-averaged ρR as a function of polar and azimuthal angle. The blue plus signs indicate the centers of the two opposing reduced-drive cones (i.e., the mode 2 axis), while the red x indicates the initial location of the stalk mount. The black circles represent the location of the ρR detectors. The imprint of the imposed mode 2 laser drive asymmetry can be clearly seen. (b) Comparison of measured (black squares) and simulated (red circles) ρR as a function of angle to the imposed mode 2 (left plus sign in panel (a)).

4. SUMMARY AND CONCLUSIONS

In this paper, we contrast measured observables to results from a 3D xRAGE simulation including capsule stalk mount for an implosion with an imposed mode 2 asymmetry, with the goal of improving our understanding of the signatures and sources of low mode asymmetries. Comprehensive comparisons are made between the simulation output and measured results, including yields, neutron emission history, neutron spectra, shell trajectory, and symmetry in time-integrated and time-resolved x-ray images and ρR.

Simulated and measured shell trajectories and mode 2 asymmetry amplitudes inferred from time-resolved x-ray images agree well, as do simulated and measured bang times and neutron emission widths, indicating that the simulation is capturing the overall hydrodynamics of the implosion.

Measured and simulated time-integrated core x-ray images clearly exhibit the signature of the imposed mode 2. The angle of the measured mode 2 deviates from the imposed mode 2 axis, suggesting that the stalk mount is distorting the asymmetry. Analysis of the simulation shows that the apparent stalk angle is shifted by 7° relative to its initial location due to interplay with the imposed mode 2. The stalk feature also appears shifted relative to its initial location in an identical way in simulated and measured time-integrated images, confirming the ability of the simulation to capture the experimental asymmetry. According to the simulation, the imposed mode 2 also distorts the location of the weak spot generated by the stalk. This is apparent in the simulated ρR distribution, which clearly shows the imprint of the mode 2, but also a weak spot due to the stalk. The trend in simulated ρR is approximately reproduced in measurements.

The most important differences between measurement and simulation are in yield and in LOS variations in apparent T_{ion} inferred from neutron spectra. The simulated yield is high, but not excessively so if compared to the experimental yield from a nominally identical shot (yield-over-simulated for this shot is 81%, see Table I and Table II). Comparing measured and simulated neutron emission histories, the difference appears to arise because the simulation is overestimating shock neutron emission. The measured LOS asymmetry in T_{ion} is not reproduced in the simulation. This asymmetry is highly sensitive to the timing of outflow along the asymmetry axis relative to peak neutron emission, and the mismatch between experiment and simulation here could potentially also be explained by the overestimated shock yield in the simulation weighting the average to earlier times. Combined, these two observations (yield and T_{ion} LOS variation differences) may point to an issue in how energy deposited by shocks is modeled in the simulation, which could be an important result.

The conclusion from earlier work that interference between the asymmetries seeded by different asymmetry seeds substantially impacts implosion dynamics is strongly supported by the new results presented here. To understand and mitigate the signatures of low modes in experiments, all asymmetry seeds must be considered.

ACKNOWLEDGEMENTS

The authors sincerely thank the OMEGA operations staff who supported this work, Bob Frankel and Ernie Doeg for processing the CR-39, Michelle Evans for characterizing the target glue spots, and Rahul Shah for helpful discussions about framing camera viewing angles. This material is based upon work supported by the Department of Energy, National Nuclear Security Administration under Award Numbers DE-NA0002949 and DE-NA0003868, by the National Laser Users' Facility under award number DE-NA0003938, by LLE under award number 417532-G, and by Los Alamos National Laboratory operated by Triad National Security for the U.S. Department of Energy NNSA under Contract No. 89233218CNA000001. This report was prepared as an account of work sponsored by an agency of the United States Government. Neither the United States Government nor any agency thereof, nor any of their employees, makes any warranty, express or implied, or assumes any legal liability or responsibility for the accuracy, completeness, or usefulness of any information, apparatus, product, or process disclosed, or represents that its use would not infringe privately owned rights. Reference herein to any specific commercial product, process, or service by trade name, trademark, manufacturer, or otherwise does not necessarily constitute or imply its endorsement, recommendation, or favoring by the United States Government or any agency thereof. The views and opinions of authors expressed herein do not necessarily state or reflect those of the United States Government or any agency thereof.

REFERENCES

[1] S. Atzeni & J. Meyer-Ter-Vehn, The Physics of Inertial Fusion, Oxford University Press (2004).

[2] O.A. Hurricane, D.A. Callahan, D.T. Casey, E.L. Dewald, T.R. Dittrich, T. Döppner, S. Haan, D.E. Hinkel, L.F. Berzak Hopkins, O. Jones, A.L. Kritcher, S. Le Pape, T. Ma, A.G. MacPhee, J.L. Milovich, J. Moody, A. Pak, H.-S. Park, P.K. Patel, J.E. Ralph, H.F. Robey, J.S. Ross, J.D. Salmonson, B.K. Spears, P.T. Springer, R. Tommasini, F. Albert, L.R. Benedetti, R. Bionta, E Bond, D.K. Bradley, J. Caggiano, P.M. Celliers, C. Cerjan, J.A. Church, R. Dylla-Spears, D. Edgell, M.J. Edwards, D. Fittinghoff, M.A. Barrios Garcia, A. Hamza, R. Hatarik, H. Herrmann, M. Hohenberger, D. Hoover, J.L. Kline, G. Kyrala, B. Kozioziemski, G. Grim, J.E. Field, J. Frenje, N. Izumi, M. Gatu Johnson, S.F. Khan, J. Knauer, T. Kohut, O. Landen, F. Merrill, P. Michel, S.R. Nagel, A. Nikroo, T. Parham, R.R. Rygg, D. Sayre, M. Schneider, D. Shaughnessy, D. Strozzi, R.P.J. Town, D. Turnbull, P. Volegov, A. Wan, K. Widmann, C. Wilde and C. Yeamans, Nature Physics 12, 800 (2016). (DOI: 10.1038/NPHYS3720)

[3] S. LePape, L. F. Berzak Hopkins, L. Divol, A. Pak, E. L. Dewald, S. Bhandarkar, L. R. Bennedetti, T. Bunn, J. Biener, J. Crippen, D. Casey, D. Edgell, D. N. Fittinghoff, M. Gatu-Johnson, C. Goyon, S. Haan, R. Hatarik, M. Havre, D. D-M. Ho, N. Izumi, J. Jaquez, S. F. Khan, G. A. Kyrala, T. Ma, A. J. Mackinnon, A. G. MacPhee, B. J. MacGowan, N. B. Meezan, J. Milovich, M. Millot, P. Michel, S. R. Nagel, A. Nikroo, P. Patel, J. Ralph, J. S. Ross, N. G. Rice, D. Strozzi, M. Stadermann, P. Volegov, C. Yeamans, C. Weber, C. Wild, D. Callahan, and O. A. Hurricane, Phys. Rev. Lett. 120, 245003 (2018).
[4] S.P. Regan, V. N. Goncharov, I. V. Igumenshchev, T. C. Sangster, R. Betti, A. Bose, T. R. Boehly, M. J. Bonino, E. M. Campbell, D. Cao, T. J. B. Collins, R. S. Craxton, A. K. Davis, J. A. Delettrez, D. H. Edgell, R. Epstein, C. J. Forrest, J. A. Frenje, D. H. Froula, M. Gatu Johnson, V. Yu. Glebov, D. R. Harding, M. Hohenberger, S. X. Hu, D. Jacobs-Perkins, R. Janezic, M. Karasik, R. L. Keck, J. H. Kelly, T. J. Kessler, J. P. Knauer, T. Z. Kosc, S. J. Loucks, J. A. Marozas, F. J. Marshall, R. L. McCrory, P.W. McKenty, D. D. Meyerhofer, D. T. Michel, J. F. Myatt, S. P. Obenschain, R. D. Petrasso, P. B. Radha, B. Rice, M. J. Rosenberg, A. J. Schmitt, M. J. Schmitt, W. Seka, W. T. Shmayda, M. J. Shoup III, A. Shvydky, S. Skupsky, A. A. Solodov, C. Stoeckl, W. Theobald, J. Ulreich, M. D. Wittman, K. M. Woo, B. Yaakobi, and J. D. Zuegel, Phys. Rev. Lett. **117**, 025001 (2016).
[5] R.H.H. Scott, D. S. Clark, D. K. Bradley, D. A. Callahan, M. J. Edwards, S.W. Haan, O. S. Jones, B. K. Spears, M. M. Marinak, R. P. J. Town, P. A. Norreys, and L. J. Suter, Phys. Rev. Lett. **110**, 075001 (2013).
[6] B.K. Spears, M.J. Edwards, S. Hatchett, J. Kilkenny, J. Knauer, A. Kritcher, J. Lindl, D. Munro, P. Patel, H.F. Robey, and R.P.J. Town, Phys. Plasmas 21, 042702 (2014).
[7] A. L. Kritcher, R. Town, D. Bradley, D. Clark, B. Spears, O. Jones, S. Haan, P. T. Springer, J. Lindl, R. H. H. Scott, D. Callahan, M. J. Edwards, and O. L. Landen, Phys. Plasmas 21, 042708 (2014).
[8] A. L. Kritcher, D. E. Hinkel, D. A. Callahan, O. A. Hurricane, D. Clark, D. T. Casey, E. L. Dewald, T. R. Dittrich, T. Döppner, M. A. Barrios Garcia, S. Haan, L. F. Berzak Hopkins, O. Jones, O. Landen, T. Ma, N. Meezan, J. L. Milovich, A. E. Pak, H.-S. Park, P. K. Patel, J. Ralph, H. F. Robey, J. D. Salmonson, S. Sepke, B. Spears, P. T. Springer, C. A. Thomas, R. Town, P. M. Celliers, and M. J. Edwards, Phys. Plasmas 23, 052709 (2016).
[9] I.V. Igumenshchev, V.N. Goncharov, F.J. Marshall, J.P. Knauer, E.M. Campbell, C.J. Forrest, D.H. Froula, V.Yu. Glebov, R.L. McCrory, S.P. Regan, T.C. Sangster, S. Skupsky and C. Stoeckl, Phys. Plasmas **23**, 052702 (2016).
[10] F.H. Séguin, C.K. Li, J.L. DeCiantis, J.A. Frenje, J.R. Rygg, R.D. Petrasso, F.J. Marshall, V. Smalyuk, V.Yu. Glebov, J.P. Knauer, T.C. Sangster, J.D. Kilkenny, and A. Nikroo, Phys. Plasmas **23**, 032705 (2016).
[11] I.V. Igumenshchev, D.T. Michel, R.C. Shah, E.M. Campbell, R. Epstein, C.J. Forrest, V.Yu. Glebov, V.N. Goncharov, J.P. Knauer, F.J. Marshall, R.L. McCrory, S.P. Regan, T.C. Sangster, C. Stoeckl, A.J. Schmitt and S. Obenschein, Phys. Plasmas 24, 056307 (2017).
[12] R.C. Shah, B.M. Haines, F.J. Wysocki, J.F. Benage, J.A. Fooks, V. Glebov, P. Hakel, M. Hoppe, I.V. Igumenshchev, G. Kagan, R.C. Mancini, F.J. Marshall, D.T. Michel, T.J. Murphy, M.E. Schoff, K. Silverstein, C. Stoeckl and B. Yaakobi, Phys. Rev. Lett. 118, 135001 (2017).
[13] A. Bose, R. Betti, D. Shvarts, and K.M. Woo, Phys. Plasmas 24, 102704 (2017).
[14] K. M. Woo, R. Betti, D. Shvarts, A. Bose, D. Patel, R. Yan, P.-Y. Chang, O. M. Mannion , R. Epstein , J. A. Delettrez, M. Charissis, K. S. Anderson, P. B. Radha, A. Shvydky, I. V. Igumenshchev, V. Gopalaswamy, A. R. Christopherson, J. Sanz, and H. Aluie, Phys. Plasmas 25, 052704 (2018).
[15] A. Bose, R. Betti, D. Mangino, K. M. Woo, D. Patel, A. R. Christopherson, V. Gopalaswamy, O. M. Mannion, S. P. Regan, V. N. Goncharov, D. H. Edgell, C. J. Forrest, J. A. Frenje , M. Gatu Johnson , V. Yu Glebov, I. V. Igumenshchev, J. P. Knauer, F. J. Marshall, P. B. Radha, R. Shah, C. Stoeckl, W. Theobald, T. C. Sangster, D. Shvarts, and E. M. Campbell, Phys. Plasmas 25, 062701 (2018).
[16] K. M. Woo, R. Betti, D. Shvarts, O. M. Mannion, D. Patel, V. N. Goncharov, K. S. Anderson, P. B. Radha, J. P. Knauer, A. Bose, V. Gopalaswamy, A. R. Christopherson, E. M. Campbell, J. Sanz, and H. Aluie, Phys. Plasmas 25, 102710 (2018).
[17] P. T. Springer, O. A. Hurricane, J. H. Hammer, R. Betti, D. A. Callahan, E. M. Campbell, D. T. Casey, C. J. Cerjan, D. Cao, E. Dewald, L. Divol, T. Doeppner, M. J. Edwards, J. E. Field, C. Forrest, J. Frenje, J. A. Gaffney, M. Gatu-Johnson, V. Glebov, V. N. Goncharov, G. P. Grim, E. Hartouni, R. Hatarik, D. E. Hinkel, L. F. B. Hopkins, I. Igumenshchev, P Knapp, J. P. Knauer, A.L. Kritcher, O. Landen, A. Pak, S. Le Pape, T. Ma, A. G. MacPhee, D. H. Munro, R. C. Nora, P. K. Patel, L. Peterson, P. B. Radha, S. P. Regan, H. Rinderknecht, C. Sangster, B. K. Spears, C. Stoeckl, Nucl. Fusion 59, 032009 (2019).
[18] M. Gatu Johnson, B.D. Appelbe, J.P. Chittenden, J. Delettrez, C. Forrest, J.A. Frenje, V.Yu. Glebov, W. Grimble, B.M. Haines, I. Igumenshchev, R. Janezic, J.P. Knauer, B. Lahmann, F.J. Marshall, T. Michel, F.H. Séguin, C. Stoeckl, C. Walsh, A.B. Zylstra, R.D. Petrasso, Phys. Rev. E 98, 051201(R) (2018).
[19] M. Gatu Johnson, B.D. Appelbe, J.P. Chittenden, A. Crilly, J. Delettrez, C. Forrest, J.A. Frenje, V.Yu. Glebov, W. Grimble, B.M. Haines, I. Igumenshchev, R. Janezic, J.P. Knauer, B. Lahmann, F.J. Marshall, T. Michel, F.H. Séguin, C. Stoeckl, C. Walsh, A.B. Zylstra, R.D. Petrasso, Phys. Plasmas 26, 012706 (2019).
[20] J.P. Chittenden, B.D. Appelbe, F. Manke, K. McGlinchey, and N.P.L. Niasse, Phys. Plasmas 23, 052708 (2016).

[21] M. Gittings, R. Weaver, M. Clover, T. Betlach, N. Byrne, R. Coker, E. Dendy, R. Hueckstaedt, K. New, W.R. Oakes, D. Ranta and R. Stefan, Comput. Sci. Discovery 1, 015005 (2008).
[22] Brian M. Haines, Gary P. Grim, James R. Fincke, Rahul C. Shah, Chad J. Forrest, Kevin Silverstein, Frederic J. Marshall, Melissa Boswell, Malcolm M. Fowler, Robert A. Gore, Anna C. Hayes-Sterbenz, Gerard Jungman, Andreas Klein, Robert S. Rundberg, Michael J. Steinkamp, and Jerry B. Wilhelmy, Phys. Plasmas 23, 072709 (2016).
[23] B.M. Haines, C.H. Aldrich, J.M. Campbell, R.M. Rauenzahn and C.A. Wingate, Phys. Plasmas 24, 052701 (2017).
[24] S.P. Lyon and J.D. Johnson, SESAME: The Los Alamos National Laboratory equation of state database, Los Alamos National Laboratory, Report No. LA-UR-92-3407, 1992.
[25] J. A. Marozas, M. Hohenberger, M. J. Rosenberg, D. Turnbull, T. J. B. Collins, P. B. Radha, P. W. McKenty, J. D. Zuegel, F. J. Marshall, S. P. Regan, T. C. Sangster, W. Seka, E. M. Campbell, V. N. Goncharov, M. W. Bowers, J.-M. G. Di Nicola, G. Erbert, B. J. MacGowan, L. J. Pelz, J. Moody, and S. T. Yang, Phys. Plasmas 25, 056314 (2018).
[26] J. Colgan, D.P. Kilcrease, N.H. Magee, M.E. Sherrill, J. Abdallah, Jr., P. Hakel, C.J. Fontes, J.A. Guzik, and K.A. Mussack, Astrophys. J. 817, 116 (2016).
[27] K.S. Anderson, C.J. Forrest, O.M. Mannion, F.J. Marshall, R.C. Shah, J.A. Marozas, P.B. Radha, D. Edgell, R. Epstein, V.N. Goncharov, J.P. Knauer, D.T. Michel, M. Gatu Johnson, and S. Laffite, "Effect of cross-beam energy transfer on target offset asymmetry in directly-driven inertial confinement fusion implosions", in preparation for submission to Phys. Plasmas (2019).
[28] B. Appelbe and J. Chittenden, Plasma Phys. Control. Fusion 53, 045002 (2011).
[29] T. J. Murphy, Phys. Plasmas 21, 072701 (2014).
[30] M. Gatu Johnson, J.P. Knauer, C.J. Cerjan, M.J. Eckart, G.P. Grim, E.P. Hartouni, R. Hatarik, J.D. Kilkenny, D.H. Munro, D.B. Sayre, B.K. Spears, R.M. Bionta, E.J. Bond, J.A. Caggiano, D. Callahan, D.T. Casey, T. Döppner, J.A. Frenje, V.Yu. Glebov, O. Hurricane, A. Kritcher, S. LePape, T. Ma, A. Mackinnon, N. Meezan, P. Patel, R.D. Petrasso, J.E. Ralph, P.T. Springer, and C.B. Yeamans, Phys. Rev. E 94, 021202(R) (2016).
[31] V.Yu. Glebov, T. C. Sangster, C. Stoeckl, J. P. Knauer, W. Theobald, K. L. Marshall, M. J. Shoup III, T. Buczek, M. Cruz, T. Duffy, M. Romanofsky, M. Fox, A. Pruyne, M. J. Moran, R. A. Lerche, J. McNaney, J. D. Kilkenny, M. J. Eckart, D. Schneider, D. Munro, W. Stoeffl, R. Zacharias, J. J. Haslam, T. Clancy, M. Yeoman, D. Warwas, C. J. Horsfield, J.-L. Bourgade, O. Landoas, L. Disdier, G. A. Chandler, and R. J. Leeper, Rev. Sci. Instrum. 81, 10D325 (2010).
[32] University of Rochester, Laboratory for Laser Energetics, National Laser Users' Facility Users Guide, http://www.lle.rochester.edu/media/about/documents/UsersGuide/05_UsersGuide.pdf (2014).
[33] V.Yu. Glebov, "Six DT nTOF detectors on OMEGA", nTOF Diagnostic Workshop, LLNL, July 18 (2017).
[34] C. Stoeckl, R. Boni, F. Ehrne, C.J. Forrest, V. Yu. Glebov, J. Katz, D.J. Lonobile, J. Magoon, S.P. Regan, M.J. Shoup III, A. Sorce, C. Sorce, T.C. Sangster and D. Weiner, Rev. Sci. Instrum. **87**, 053501 (2016).
[35] W. Grimble, F.J. Marshall, and E. Lambrides, Phys. Plasmas **25**, 072702 (2018); LLE Review, Vol. 151, p.146-151 (2017).
[36] M. Gatu Johnson, P.J. Adrian, K.S. Anderson, B.D. Appelbe, J.P. Chittenden, A.J. Crilly, D. Edgell, C.J. Forrest, J.A. Frenje, V.Yu. Glebov, B.M. Haines, I. Igumenshchev, D. Jacobs-Perkins, R. Janezic, N.V. Kabadi, J.P. Knauer, B. Lahmann, O.M. Mannion, F.J. Marshall, T. Michel, F.H. Séguin, R. Shah, C. Stoeckl, C.A. Walsh, and R.D. Petrasso, Phys. Plasmas **27**, 032704 (2020).
[37] M. Gatu Johnson, D.T. Casey, J.A. Frenje, C.-K. Li, F.H. Séguin, R.D. Petrasso, R. Ashabranner, R. Bionta, S. LePape, M. McKernan, A. Mackinnon, J.D. Kilkenny, J. Knauer and T.C. Sangster, Phys. Plasmas 20, 042707 (2013).
[38] L. Ballabio, J. Källne, and G. Gorini, Nucl. Fusion 38, 1723 (1998).
[39] D.T. Michel, A.K. Davis, W. Armstrong, R. Bahr, R. Epstein, V.N. Goncharov, M. Hohenberger, I.V. Igumenshchev, R. Jungquist, D.D. Meyerhofer, P.B. Radha, T.C. Sangster, C. Sorce and D.H. Froula, High Power Laser Science and Engineering 3, e19 (2015). doi:10.1017/hpl.2015.15
[40] F.J. Marshall, J.A. Oertel, Rev. Sci. Instrum. 68, 735 (1997).
[41] A.L. Velikovich, K.G. Whitney, and J.W. Thornhill, Phys. Plasmas **8**, 4524 (2001).
[42] D. T. Casey, J. A. Frenje, M. Gatu Johnson, F. H. Séguin, C. K. Li, R. D. Petrasso, V. Yu. Glebov, J. Katz, J. Magoon, D. D. Meyerhofer, T. C. Sangster, M. Shoup, J. Ulreich, R. C. Ashabranner, R. M. Bionta, A. C. Carpenter, B. Felker, H. Y. Khater, S. LePape, A. MacKinnon, M. A. Mckernan, M. Moran, J. R. Rygg, M. F. Yeoman, R. Zacharias, R. J. Leeper, K. Fletcher, M. Farrell, D. Jasion, J. Kilkenny, and R. Paguio, Rev. Sci. Inst. **84**, 043506 (2013).
[43] D. Hicks, "Charged-Particle Spectroscopy: A new window on Inertial Confinement Fusion", PhD Thesis, Massachusetts Institute of Technology (1999).
[44] F. H. Séguin, J. A. Frenje, C. K. Li, D. G. Hicks, S. Kurebayashi, J. R. Rygg, B.-E. Schwartz, R. D. Petrasso, S. Roberts, J. M. Soures, D. D. Meyerhofer, T. C. Sangster, J. P. Knauer, C. Sorce, V. Yu. Glebov, C. Stoeckl, T. W. Phillips, R. J. Leeper, K. Fletcher and S. Padalino, Rev. Sci. Instrum. 74, 975 (2003).